

# Copper Complexes with Carbon-Related Radiation Defects in Silicon

Nikolai Yarykin,<sup>\*</sup> Jörg Weber, Stanislau Lastovskii, and Vasilii Gusakov

**Experimental and theoretical study of the interaction of mobile interstitial copper with the dominant carbon-related radiation defects in Si is presented. The deep-level transient spectroscopy measurements detect a passivation of the  $C_i$  and  $C_iO_i$  centers due to the formation of complexes with  $Cu_i$  at room temperature. Both the Cu–C and Cu–CO complexes have equal dissociation energy of  $1.07 \pm 0.02$  eV and close preexponential factors. Equilibrium structures, formation energies, and dissociation barriers for the Cu–C and Cu–CO complexes are determined by ab initio calculations performed within the framework of the density functional approach. Theory predicts that the  $C_i$  and  $C_iO_i$  defects basically retain their structures upon capture of a copper atom that is located near the carbon atoms in both cases. The calculated dissociation barriers are in good agreement with the experiment.**

The copper interaction with interstitial-type defects, which is the topic of the present work, is less studied. The ab initio calculations predicted that copper can form a complex with self-interstitials.<sup>[11]</sup> However, such reaction seems to be kinetically prohibited in p-type Si.<sup>[7]</sup> The interstitial carbon species  $C_i$  were experimentally shown to lose their electrical activity due to the formation of Cu–C complexes.<sup>[7,8]</sup> The complexes dissociate with an activation energy of  $\approx 1$  eV that is essentially higher than the diffusion barrier for isolated  $C_i$  ( $\approx 0.75$  eV).<sup>[12,13]</sup> Therefore, formation of the Cu–C complexes retards the standard  $C_i$  reactions and an accurate determination of the Cu–C dissociation energy is one of the purposes of the current work.

## 1. Introduction

Detrimental copper contamination of Si wafers, usually in the form of highly mobile  $Cu_i$  species, can occur during various technological processes. In contrast, radiation defects are created intentionally by irradiation of the wafers with energetic particles to control the lifetime of minority carriers or unintentionally by plasma etching. Interaction of copper with radiation defects is the subject of several works.<sup>[1–10]</sup> Evolution of the vacancy-type defects is understood rather well: The final defect spectrum strongly depends on the copper contamination level.<sup>[10]</sup> The dominant vacancy-type radiation defect, VO, is transformed into the CuVO complex under the conditions of low copper concentration.<sup>[6]</sup> When the  $Cu_i$  concentration is high, the primary vacancies are consumed in the reaction with  $Cu_i$  and the VO and CuVO complexes are not formed.<sup>[9]</sup>

The available information on the copper interaction with another carbon-related radiation defect (namely, the  $C_iO_i$  pair which prevails in the oxygen-rich Cz-grown Si), is rather scant and contradictory. Essential decrease of the  $C_iO_i$  concentration was demonstrated due to copper introduction into irradiated Si at room temperature.<sup>[2]</sup> In contrast, the  $C_iO_i$  concentration remained constant at 350 K under conditions in which presence of mobile copper was confirmed by formation of the CuVO complexes.<sup>[5]</sup> In this work, we show that the Cu–CO complex of limited thermal stability does exist.

This study considers an artificial situation of a rather high copper contamination level. However, our results are applicable to conditions encountered in the process of device manufacturing.

## 2. Results

### 2.1. Arrangement of the Experiment


Radiation defects were introduced at room temperature into p-type Si wafers ( $[B] \approx 10^{15} \text{ cm}^{-3}$ ) containing  $\approx 3 \times 10^{14} \text{ cm}^{-3}$  mobile  $Cu_i$  species, which corresponds to a high level of copper contamination.<sup>[10]</sup> (For the preparation of Cu-doped wafers and measurements of the  $Cu_i$  concentration, see Section 6.) Accordingly, the irradiation-induced vacancies were transformed first to  $Cu_s$  and then to the  $Cu_{PL}$  centers.<sup>[9]</sup> The irradiation reduced the  $Cu_i$  concentration, which, however, remained rather high ( $\approx 10^{14} \text{ cm}^{-3}$ ).

The experimental approach was mainly based on the control of the  $Cu_i$  concentration under the Schottky diode due to annealing of the diode under reverse or zero bias. In addition to the obvious influence on the charge state of the electrically active defects with

Dr. N. Yarykin  
Institute of Microelectronics Technology RAS  
Chernogolovka 142432, Russia  
E-mail: NAY@iptm.ru

Prof. J. Weber  
Technische Universität Dresden  
Dresden 01062, Germany

Dr. S. Lastovskii, Dr. V. Gusakov  
Scientific-Practical Materials Research Center of NAS of Belarus  
Minsk 220072, Belarus

 The ORCID identification number(s) for the author(s) of this article can be found under <https://doi.org/10.1002/pssa.202100141>.

DOI: 10.1002/pssa.202100141

levels in the lower part of the gap, the  $\text{Cu}_i$  drift/diffusion is affected by the electric field of the space-charge region (SCR). The bias applied at room temperature sweeps the mobile copper out of the SCR in less than 1 s in our boron-doped samples.<sup>[14,15]</sup> Thus, annealing under reverse bias (RBA) prevents a recapture of the  $\text{Cu}_i$  species, which could appear inside the SCR due to dissociation of copper-related complexes. In contrast, short-circuiting of the diode results in flooding the former SCR (of  $\approx 5 \mu\text{m}$  width) with mobile copper from the sample volume in a few seconds at room temperature.<sup>[15]</sup> Thus, copper-related complexes could be formed again.

## 2.2. Cu–CO Complex

The  $\text{C}_i\text{O}_i$  centers and divacancies with donor levels at  $E_v + 0.36$  and  $E_v + 0.19$  eV, respectively, are the dominant defects observed by the deep-level transient spectroscopy (DLTS) technique in the Cu-free irradiated p-type oxygen-rich Cz–Si crystals.<sup>[16,17]</sup> ( $E_v$  stands for the top of the valence band.) However, neither of these defects nor  $\text{C}_i$  (the  $\text{C}_i\text{O}_i$  precursor) was detected in our as-irradiated Cu-contaminated samples. The absence of these standard radiation defects was earlier reported in oxygen-lean FZ–Si samples with a similar level of copper contamination.<sup>[7,8]</sup> In that case, the appearance of the  $\text{C}_i$  center due to RBA at 320–340 K was attributed to the dissociation of a passive Cu–C pair. First RBA experiments on the as-irradiated Cz–Si samples showed that annealing at near room temperature resulted in the appearance of a DLTS signal at  $\approx 190$  K, which could be interpreted as the  $\text{C}_i\text{O}_i$  donor level. However, investigations on the as-irradiated samples are complicated by the fact that the carbon–oxygen pairs appear in two forms,  $\text{C}_i\text{O}_i$  and  $\text{C}_i\text{O}_i^*$ , with strongly overlapping DLTS peaks.<sup>[18,19]</sup> Furthermore, the DLTS peak of the bistable center attributed to a  $\text{IO}_{2i}$  complex appears at almost the same temperature.<sup>[20,21]</sup> To avoid these problems, the irradiated Cz–Si samples (without diodes) were annealed at 450 K for 30 min. Such treatment is known to transform  $\text{C}_i\text{O}_i^*$  into  $\text{C}_i\text{O}_i$  and removes the bistable complexes.<sup>[18,22]</sup> The  $\text{Cu}_i$  concentration decreased somewhat as a result of the annealing but remained higher than the expected concentration of the  $\text{C}_i\text{O}_i$  centers ( $\approx 4 \times 10^{13} \text{ cm}^{-3}$ ).

Still, no standard radiation defects were revealed in such crystals (Figure 1, blue dashed curve), while the DLTS spectrum of the Cu-free irradiated samples annealed at  $\approx 450$  K was dominated by the divacancy and  $\text{C}_i\text{O}_i$  peaks (not shown).

The  $\text{H}_{71}$  peak of unknown nature regularly appears in the irradiated Cu-diffused Cz–Si crystals. The strong signal at  $\approx 50$  K (not shown) is determined by the  $\text{Cu}_{\text{PL}}$  center that was formed as a result of copper indiffusion and then strongly increased due to the electron irradiation.<sup>[9]</sup> Presence of this signal is an indication of the high  $\text{Cu}_i$  concentration during the irradiation.<sup>[10]</sup> This signal is rather stable during the treatments considered subsequently and will not be discussed further.

The RBA treatments of such samples in the temperature range of 290–340 K result in the appearance of the DLTS peak at 192 K (Figure 1). The emission parameters of the corresponding defect were undistinguishable from those for the  $\text{C}_i\text{O}_i$  center in Cu-free irradiated crystals. The  $\text{C}_i\text{O}_i$  centers were only formed inside the SCR existed during RBA (see the inset in Figure 1), while the

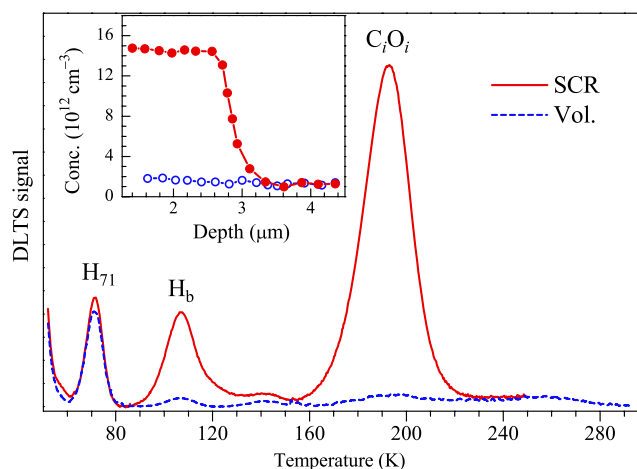


**Figure 1.** DLTS spectra of the copper-doped irradiated Cz–Si after heat treatment at 450 K for 30 min (blue dashed curve) and after additional annealing at 320 K for 10 min inside the SCR (red solid curve). Rate window  $49 \text{ s}^{-1}$ . In the inset are depth profiles of the  $\text{C}_i\text{O}_i$  center before (blue open symbols) and after the 320 K annealing under the reverse bias of 4 V (red dots).

deep-level spectrum in the quasi-neutral region remained invariable. The peak at 107 K corresponds to the  $\text{H}_b$  defect, which was formed due to the copper indiffusion and was activated by removing the mobile copper.<sup>[23]</sup> Note that no divacancy signal (expected at  $\approx 115$  K) appeared in the Cu-contaminated samples.

The newly formed  $\text{C}_i\text{O}_i$  signal could be totally bleached by flooding the near-surface layer with mobile copper in the short-circuited diode. The following RBA treatment revealed the  $\text{C}_i\text{O}_i$  pairs again. This cycle can be repeated many times as long as the  $\text{Cu}_i$  concentration remains high enough. Such behavior evidences the formation of a Cu–CO complex without any deep level in the lower half of the gap. The complexes form in the short-circuited diode and dissociate under the reverse bias remaining the  $\text{C}_i\text{O}_i$  centers.

The kinetics of the  $\text{C}_i\text{O}_i$  appearance (i.e., the Cu–CO dissociation) during the isothermal reverse-bias annealings at 320 and 335 K were measured as follows. First, the  $\text{C}_i\text{O}_i$  centers were totally passivated by flooding the near-surface layer with mobile copper at room temperature. Afterward, the sample was cooled down to 192 K (the  $\text{C}_i\text{O}_i$  peak position) under zero bias and the reference DLTS signal was estimated. Then, under the applied reverse bias of 4 V, the sample was heated to 320 K (335 K), kept for a certain time, and cooled again to measure the  $\text{C}_i\text{O}_i$  concentration at the depth of 1.4–2.6  $\mu\text{m}$  (see the inset in Figure 1). Such annealing steps were repeated several times until the  $\text{C}_i\text{O}_i$  concentration reached its maximum value, which was practically equal to the  $\text{C}_i\text{O}_i$  concentration in the Cu-free samples irradiated with the same fluence. The  $\text{C}_i\text{O}_i$  concentration in the sample shown in Figure 1 reached  $\approx 4 \times 10^{13} \text{ cm}^{-3}$  after a long enough RBA treatment.

The red dots and circles in Figure 2 are perfectly fitted by straight lines, indicating that the  $\text{C}_i\text{O}_i$  center appearance is well described by first-order kinetics. The line slopes give the characteristic times of 28 and 5.4 min at 320 and 335 K, respectively.

Note that the abscissa scale in Figure 2 indicates the *effective* RBA time, which takes into account that the annealing starts already during heating up to the annealing temperature and continues for some time during cooling. The used approach is described in the **Appendix**. Based on these two isothermal anneals, the process rates at other temperatures were measured using a single annealing step of appropriate duration after the total  $C_iO_i$  passivation. The corrections for the effective annealing time were also applied. The rates determined for the interval of 292–335 K are perfectly fitted by a straight line in the Arrhenius plot (**Figure 3**). The slope and position of the line correspond to the activation energy of 1.06 eV and the preexponential factor of  $2.5 \times 10^{13} \text{ s}^{-1}$ .

### 2.3. Cu–C Complex

The bleaching of the  $C_i$  donor level by flooding the near-surface layer with mobile copper and its reappearance due to the following RBA treatment were earlier observed in FZ–Si copper-contaminated irradiated samples.<sup>[7,8]</sup> However, the activation energy of the process was only roughly estimated. Therefore, we repeated those experiments with a special attention to the kinetics of  $C_i$  formation. The approach used was similar to that described above for the  $C_iO_i$  centers.

Increase of the  $C_i$  concentration during the isothermal annealing under reverse bias at 315 K is shown in Figure 2 (black triangles). The points obtained with the  $C_i$  saturation level  $S_0 = 4.2 \times 10^{13} \text{ cm}^{-3}$  are well described by first-order kinetics. The temperature dependence of the Cu–C dissociation rate is shown in Figure 3 with black triangles. The parameters of the process are shown in the figure.

## 3. Discussion

It was argued<sup>[7,8]</sup> that  $C_i$  defects are formed in copper-contaminated electron-irradiated Si in a standard way via Watkins' replacement

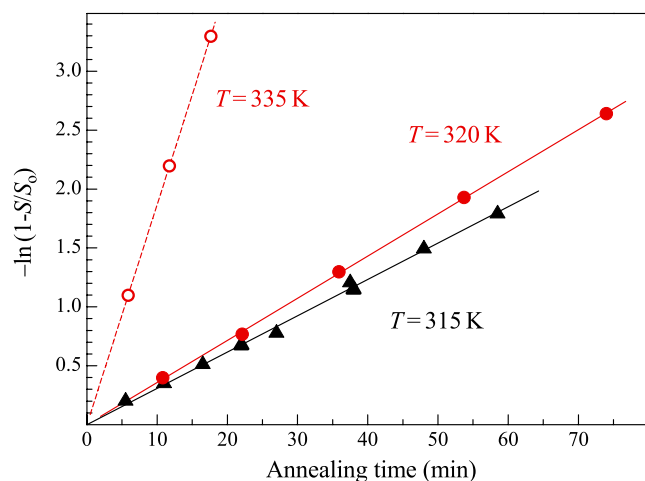


**Figure 2.** Appearance of the  $C_iO_i$  pairs in Cz–Si (red dots and circles) and of the  $C_i$  centers in FZ–Si crystals (black triangles) during isothermal annealing inside the SCR at the indicated temperatures.  $S$  and  $S_0$  are the current and maximum amplitudes of the  $C_iO_i$  or  $C_i$  DLTS signals, respectively.

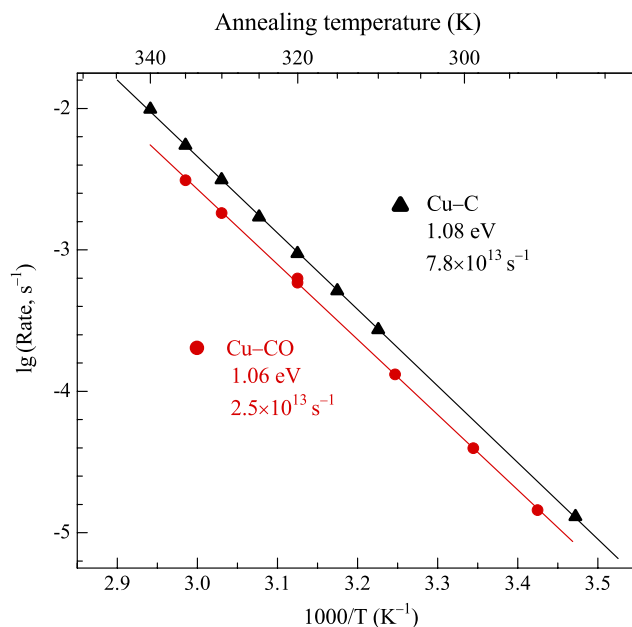


**Figure 3.** Arrhenius plot for the dissociation rates of the Cu–CO complexes in Cz–Si (red dots) and of the Cu–C pairs in FZ–Si (black triangles) during anneals under reverse bias.

mechanism. As soon as the  $C_i$  center acquires the neutral-charge state, it is attacked by the mobile  $Cu_i^+$  species. Taking into account the  $C_i$  donor level position,<sup>[17,24]</sup> and boron and  $Cu_i$  concentrations in our samples, this happens in less than 1 s. This consideration remains valid for the Cz–Si samples since it takes minutes at room temperature for  $C_i$  to diffuse to oxygen atoms and form  $C_iO_i$  in copper-free oxygen-rich crystals.<sup>[17]</sup>

Dissociation of the Cu–C complex can be detected in our experiments only inside the SCR of the reverse-biased diodes. Taking into account that the Cu–C pair possesses no level in the lower half of the bandgap, the effect of bias has to be totally attributed to the fact that the SCR electric field effectively removes the released  $Cu_i$  species. The remaining  $C_i$  atoms are neutral inside the SCR, diffuse in the normal way, and form  $C_iO_i$  and other complexes.

In the quasi-neutral region, the Cu–C association is orders of magnitude faster than the dissociation. Therefore, it is rather questionable if the  $C_iO_i$  centers are formed even in the oxygen-rich Cz–Si during the zero-bias annealing at relatively low temperatures (e.g., 340 K). However, the Cu–C dissociation rate (Figure 3) and the  $C_i$  diffusivity<sup>[12,24]</sup> quickly increase at higher temperatures and the  $C_iO_i$  pairs are expected to form in Cz–Si due to annealing at 450 K.

The repeated appearance/disappearance of the  $C_iO_i$  centers due to the reverse- or zero-bias treatments, respectively, clearly show that formation/dissociation of Cu–CO complexes takes place. The Cu–CO dissociation is  $\approx 1.6$  times slower than the Cu–C dissociation in the temperature range of 290–340 K (Figure 3). This distinction indicates that two different processes were measured, although the activation energies coincide within the experimental accuracy. The similar dissociation rates could be intuitively understood if the copper

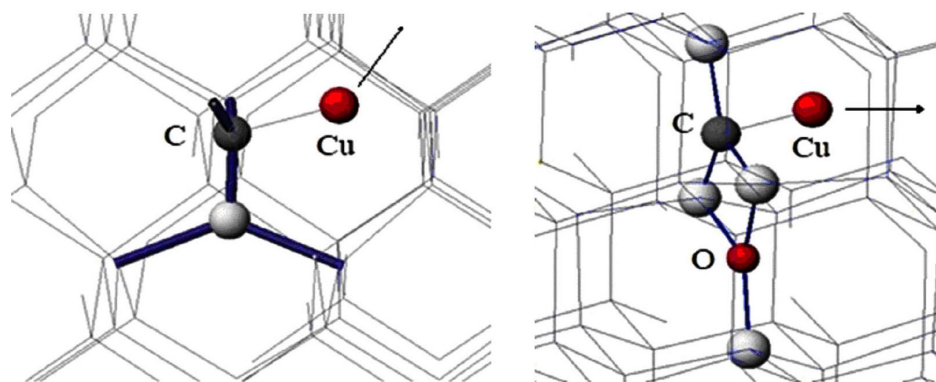


**Figure 4.** Calculated equilibrium structures of the Cu–C and Cu–CO complexes. The arrows indicate the directions of dissociation.

atom in the Cu–C and Cu–CO complexes is attached to the carbon atom.

#### 4. Ab Initio Calculations

To verify the aforementioned assumption, first-principles density-functional calculations were conducted using the Quantum ESPRESSO package.<sup>[25]</sup> The host crystal was represented by a 216 Si atom periodic supercell. A  $2 \times 2 \times 2$  Monkhorst–Pack mesh was used to sample the Brillouin zone.<sup>[26]</sup> All calculations were performed in the Perdew–Burke–Ernzerhof (PBE) approximation using the PAW pseudopotentials. A plane-wave energy cutoff of 300 eV was held constant for all the calculations.

The calculations of equilibrium structures of the Cu–C and Cu–CO complexes were conducted as follows. First of all, the equilibrium configurations of the copper-free  $C_i$  and  $C_iO_i$  defects were found at the given level of theory. These configurations agreed well with earlier findings.<sup>[27,28]</sup> To determine the equilibrium structures of the Cu–C (Cu–CO) complexes, a copper atom was placed at different interstitial positions in the first or second coordination spheres of the  $C_i$  ( $C_iO_i$ ) defects. Then, the total energy of the supercell was minimized over the coordinates of all atoms. For both defects, the structures of minimum energy were found to possess the Cu atom in the vicinity of the carbon atom (**Figure 4**). The calculated formation energies  $E_f$  are equal to 0.78 and 0.66 eV for the Cu–C and Cu–CO defects, respectively. Other defect parameters are shown in **Table 1**.

The calculations revealed also several metastable configurations. The metastable structure of the Cu–C complex with the highest binding energy of 0.4 eV corresponds to localization of the copper

atom in the vicinity of the silicon atom of the C–Si dumbbell. In case of the Cu–CO complex, placing the copper atom in the vicinity of the oxygen atom results in binding energy of  $\approx 0.3$  eV.

The energy barriers for dissociation of the most stable configurations of the Cu–C and Cu–CO complexes were calculated by displacing the copper atom to the nearest tetrahedral interstitial site as shown by the arrows in **Figure 4**. For this purpose, the total supercell energy was minimized by adjusting the coordinates of copper and several adjacent atoms under the condition that the distance  $d$  of the copper atom from its equilibrium position was equal to a given value.<sup>[29,30]</sup> The obtained dependences of the total energy  $E(d)$  are shown in **Figure 5**.

Indeed, the similar structures (Cu location close to carbon atom) result in close dissociation barriers, the absolute values of which are in a good agreement with the experiment (see **Table 1**).

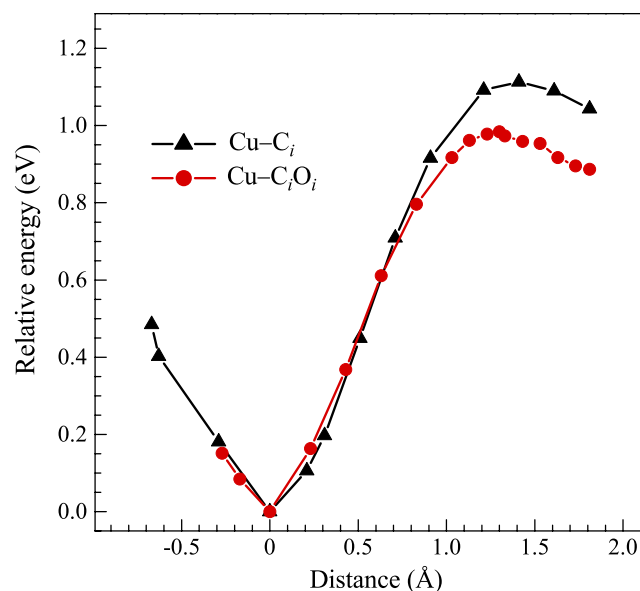


**Figure 5.** The calculated dependences of the relative energies of the supercell as a function of the Cu atom displacement along the dissociation pathway. The negative displacements correspond to movement of the Cu atom toward the C atom.

**Table 1.** Formation energy  $E_f$ , dissociation barrier  $E_b$ , and distance  $d_0$  between the copper and carbon atoms for the calculated equilibrium structures of the Cu–C and Cu–CO complexes. The experimental values are shown in brackets.

Defect	$E_f$ [eV]	$E_b$ [eV]	$d_0$ [Å]
Cu–C	0.78	1.1 [1.08]	2.088
Cu–CO	0.66	1.0 [1.06]	2.08

The calculated  $E(d)$  dependences can be used to compare the preexponential factors (prefactors) for the thermally activated dissociation of the Cu–C and Cu–CO complexes. The prefactors depend on the number of equivalent pathways for dissociation and on the shape of the potential surfaces around the equilibrium and saddle points.<sup>[31]</sup> The defect symmetries dictate that the number of equivalent pathways is twice as high for the Cu–C defect. Taking into account the small differences between the two  $E(d)$  functions in Figure 5, the prefactor is expected to be 1.8 times higher for the Cu–C complex. This value is in a fairly good agreement with the experiment: Considering the uncertainties in the experimentally measured activation energies, the ratio of the prefactors can be in the range from 1.4 to 6.1.

## 5. Conclusion

The mobile interstitial Cu<sub>i</sub> species are shown to form complexes with the C<sub>i</sub> and C<sub>i</sub>O<sub>i</sub> radiation defects, which results in the disappearance of the C<sub>i</sub> and C<sub>i</sub>O<sub>i</sub> donor levels. The Cu–C and Cu–CO complexes release the copper atoms in the temperature range of 290–340 K with activation energies of 1.06–1.08 eV. The striking similarity of the dissociation kinetics implies a likeness of the defect structures. Indeed, the ab initio calculations show that the highest binding energies of Cu–C and Cu–CO complexes in the range of 0.7–0.8 eV are achieved by placing the copper atoms to the interstitial positions in the vicinity of a carbon atom for both complexes. The theoretically estimated dissociation barriers for these most stable configurations are in good agreement with the experimental values.

## 6. Experimental Section

The start materials for the study were commercially available Cz– and FZ–Si wafers of p-type conductivity doped with boron ( $[B] = (0.6\text{--}1.1) \times 10^{15} \text{ cm}^{-3}$ ). The oxygen concentration  $[O_i]$  in the Cz–Si crystals was in the range of  $(0.7\text{--}1.0) \times 10^{18} \text{ cm}^{-3}$ , while the carbon concentration in all samples and  $[O_i]$  in FZ–Si were below  $3 \times 10^{16} \text{ cm}^{-3}$ .

Copper was introduced by a 20 min annealing at 730 °C in quartz ampoules that were intentionally contaminated with copper. The treatment was terminated by quenching into liquid nitrogen. After Mesli and Heiser,<sup>[23]</sup> the concentration of mobile copper was equal to the amplitude of a step in the CV profile measured at low temperature after cooling the Schottky diode under a fixed reverse bias. The diffusion results were found to be very sensitive to the quenching details with the mobile copper concentrations varying in the range of  $(1\text{--}5) \times 10^{14} \text{ cm}^{-3}$ . The Cu<sub>i</sub> concentration essentially reduced on the time scales of a few days at room temperature or a couple of weeks at –15 °C. Only the samples with  $[Cu_i] \geq 3 \times 10^{14} \text{ cm}^{-3}$  were used for further irradiation.

The copper-diffused samples (as well as the initial Cu-free wafers) were irradiated with 3.5 MeV electrons to  $5 \times 10^{14} \text{ cm}^{-2}$  fluence. To avoid unwanted heating under the electron beam, the samples were mounted on a water-cooled metal block. After irradiation, the samples were stored in a refrigerator at –15 °C.

All Schottky contacts were deposited after chemical etching in standard CP4 acid solution. A 1 MHz test signal was used in the DLTS and CV measurements.

## Appendix: The Annealing Duration with Finite Heating/Cooling Rates

Consider a first-order process with activation energy  $E$  and rate  $\nu_0$  at the desired annealing temperature  $T_0$ . The *effective* annealing time is defined by the equation

$$\nu_0 t^{\text{eff}} = \nu(T)t \quad (1)$$

In words, the annealing of duration  $t$  at arbitrary temperature  $T$  is equivalent to the annealing at  $T_0$  for  $t^{\text{eff}}$  time. For definiteness, consider the cooling from  $T_0$  with a constant rate  $b_c$ :  $T = T_0 - b_c t$ . (The heating stage can be considered similarly.) Using Equation (1) in the differential form, we get

$$t_c^{\text{eff}} = \int_0^\infty \frac{\nu(T)}{\nu_0} dt = \int_0^\infty \exp\left(\frac{E}{T_0} - \frac{E}{T}\right) dt \quad (2)$$

where  $t_c^{\text{eff}}$  is the total effective annealing time accumulated during cooling. This integral cannot be expressed in elemental function for the linear  $T(t)$  dependence. Because of a strong (exponential)  $\nu(T)$  dependence, only the temperatures close to  $T_0$  make a significant contribution to  $t^{\text{eff}}$ . Therefore, we linearize the expression in parentheses with respect to  $x = T - T_0$  and switch to integration over  $x$

$$t_c^{\text{eff}} = b_c^{-1} \int_{-\infty}^0 \exp\left(\frac{E}{T_0^2} x\right) dx = \frac{T_0^2}{b_c E} \quad (3)$$

This value (as well as  $t_h^{\text{eff}}$  accumulated during heating) has to be added to the nominal annealing time at  $T_0$ . This formula contains  $E$  which, generally speaking, is unknown before the experiment. Therefore, a few iteration steps are probably required.

As an example close to the real experimental parameters, Equation (3) predicts  $t_c^{\text{eff}} = 50$  s for cooling from 340 K with the rate of 0.2 K/s if the process activation energy is equal to 1 eV. Digital integration of Equation (2) gives a bit lower value of 47 s.

## Acknowledgements

This study was supported in part by the Deutsche Forschungsgemeinschaft under Contract No. WE 1319/19. The work in IMT RAS was performed in frames of the state task No 075-00355-21-00. V.G. is thankful for the support from the BRFFR project No F20MC-002.

## Conflict of Interest

The authors declare no conflict of interest.

## Data Availability Statement

The data that support the findings of this study are available from the corresponding author upon reasonable request.



## Keywords

ab initio theory, complex dissociation, copper impurities, radiation defects, silicon crystals

Received: March 14, 2021

Revised: May 26, 2021

Published online:

- [1] S. J. Pearton, A. J. Tavendale, *J. Appl. Phys.* **1983**, 54, 1375.
- [2] M. O. Aboelfotoh, B. G. Svensson, *Phys. Rev. B* **1995**, 52, 2522.
- [3] V. P. Markevich, A. R. Peaker, I. F. Medvedeva, V. Gusakov, L. I. Murin, B. G. Svensson, *Solid State Phenom.* **2008**, 131–133, 363.
- [4] L. I. Murin, I. F. Medvedeva, V. P. Markevich, *Inorganic Mater.* **2010**, 46, 333.
- [5] N. Yarykin, J. Weber, *Semiconductors* **2010**, 44, 983.
- [6] N. Yarykin, J. Weber, *Phys. Rev. B* **2011**, 83, 125207.
- [7] N. Yarykin, J. Weber, *Semiconductors* **2015**, 49, 712.
- [8] N. Yarykin, J. Weber, *Solid State Phenom.* **2016**, 242, 302.
- [9] N. Yarykin, J. Weber, *Solid State Phenom.* **2016**, 242, 308.
- [10] N. Yarykin, J. Weber, *Phys. Stat. Sol. C* **2017**, 14, 1600267.
- [11] D. West, S. K. Estreicher, S. Knack, J. Weber, *Phys. Rev. B* **2003**, 68, 035210.
- [12] L. W. Song, X. D. Zhan, B. W. Benson, G. D. Watkins, *Phys. Rev. B* **1990**, 42, 5765.
- [13] L. F. Makarenko, M. Moll, F. P. Korshunov, S. B. Lastovskii, *J. Appl. Phys.* **2007**, 101, 113537.
- [14] T. Heiser, A. Mesli, *Appl. Phys. A* **1993**, 57, 325.
- [15] A. A. Istratov, C. Flink, H. Hieslmair, E. R. Weber, T. Heiser, *Phys. Rev. Lett.* **1998**, 81, 1243.
- [16] Y. H. Lee, L. J. Cheng, J. D. Gerson, P. M. Mooney, J. W. Corbett, *Solid State Commun.* **1977**, 21, 109.
- [17] C. A. Londos, *Phys. Rev. B* **1988**, 37, 4175.
- [18] L. I. Khirunenko, Y. V. Pomozev, N. A. Tripachko, M. G. Sosnin, A. Duvanskii, L. I. Murin, J. L. Lindström, S. B. Lastovskii, L. F. Makarenko, V. P. Markevich, A. R. Peaker, *Solid State Phenom.* **2005**, 108–109, 261.
- [19] L. F. Makarenko, F. P. Korshunov, S. B. Lastovskii, L. I. Murin, M. Moll, I. Pintilie, *Semiconductors* **2014**, 48, 1456.
- [20] V. P. Markevich, L. I. Murin, S. B. Lastovskii, I. F. Medvedeva, B. A. Komarov, J. L. Lindström, A. R. Peaker, *J. Phys.: Condens. Matter* **2005**, 17, S2331.
- [21] V. P. Markevich, L. I. Murin, S. B. Lastovskii, I. F. Medvedeva, J. L. Lindström, A. R. Peaker, J. Coutinho, R. Jones, V. J. B. Torres, S. Öberg, P. R. Briddon, *Solid State Phenom.* **2005**, 108–109, 273.
- [22] N. Yarykin, J. Weber, *Physica B* **2007**, 401–402, 483.
- [23] A. Mesli, T. Heiser, *Phys. Rev. B* **1992**, 45, 11632.
- [24] S. B. Lastovskii, V. E. Gusakov, V. P. Markevich, A. R. Peaker, H. S. Yakushevich, F. P. Korshunov, L. I. Murin, *Phys. Stat. Sol. A* **2017**, 214, 1700262.
- [25] P. Giannozzi, O. Andreussi, T. Brumme, O. Bunau, M. B. Nardelli, M. Calandra, R. Car, C. Cavazzoni, D. Ceresoli, M. Cococcioni, N. Colonna, I. Carnimeo, A. D. Corso, S. de Gironcoli, P. Delugas, R. A. DiStasio, A. Ferretti, A. Floris, G. Fratesi, G. Fugallo, R. Gebauer, U. Gerstmann, F. Giustino, T. Gorni, J. Jia, M. Kawamura, H.-Y. Ko, A. Kokalj, E. Küçükbenli, M. Lazzeri, M. Marsili, N. Marzari, F. Mauri, N. L. Nguyen, H.-V. Nguyen, A. O. de-la Roza, L. Paulatto, S. Poncé, D. Rocca, R. Sabatini, B. Santra, M. Schlipf, A. P. Seitsonen, A. Smogunov, I. Timrov, T. Thonhauser, P. Umari, N. Vast, X. Wu, S. Baroni, *J. Phys.: Condens. Matter* **2017**, 29, 465901.
- [26] H. J. Monkhorst, J. D. Pack, *Phys. Rev. B* **1976**, 13, 5188.
- [27] J. Coutinho, R. Jones, P. R. Briddon, S. Öberg, L. I. Murin, V. P. Markevich, J. L. Lindström, *Phys. Rev. B* **2002**, 65, 014109.
- [28] D. Backlund, S. Estreicher, *Physica B: Condensed Matter* **2007**, 401–402, 163.
- [29] V. Gusakov, *Mater. Res. Soc. Symp. Proc.* **2005**, 864, 920.
- [30] V. E. Gusakov, *Solid State Phenom.* **2014**, 205–206, 171.
- [31] P. Hänggi, P. Talkner, M. Borkovec, *Rev. Mod. Phys.* **1990**, 62, 251.